J Mater Sci (2007) 42:1096–1107
DOI 10.1007/s10853-006-1369-9

Tensile strength degradation of ceramic fibres due to cyclic loading

F. Kaya

Received: 22 September 2005 / Accepted: 23 February 2006 / Published online: 15 January 2007

Abstract Interfacial strength of Ti β 21S/SCS 6 composite was increased via ageing. Composite specimens with a_o/W ratios of 0.24 and 0.07 were prefatigued in three point bending at ambient and at 500 °C both in the air and vacuum. Bridging fibres were extracted from the pre-fatigued specimens and tested in tensile loading to monitor the strength degradation due repeated opening and closing of the fatigue crack. A tri-modal Weibull distribution was employed to express strength distribution of the SCS 6 fibres. Results have shown that cyclic loading of the composites lower the mean tensile strength of the fibres by 20%, compared to the unfatigued composite. A marked effect of initial unbridged defect size was observed, when the tensile strength data were divided into two sub-population using the fatigue crack length values. Compared to unfatigued composite, tensile strength reductions of 41 and 22% were measured from the prefatigued composites with a_o/W of 0.24 and 0.07, respectively.

Introduction

SiC fibre reinforced Ti matrix composites have potential for use in the aerospace industry because of their high specific stiffness and strength at room and elevated temperatures. They exhibit better performance under more severe loads and environments in comparison to monolithic materials and their properties can be tailored to the specific needs. The combination of all these factors prompted these materials to be considered for high performance aerospace applications. Titanium based metal matrix composites also exhibit an interesting fatigue crack growth behaviour, where the fatigue crack growth rate, da/dN is observed to decrease with the increased crack length, whereas the fatigue crack growth of the monolithic titanium alloys can be represented by the Paris–Erdogan relationship, where rapid crack growth rate (leading to rupture of the component) is observed above a critical crack length [1]. A closer microstructural inspection reveal that this phenomenon is caused by the intact ceramic fibres within the fatigue crack wake, which serve to decrease the effective stress intensity at the growing crack tip, ΔK_{eff}. It is also observed that if the bridging fibres do not fail in the crack wake, then the fatigue crack growth rates decrease eventually to crack arrest [1]. The balance between the sub-critical crack growth and catastrophic failure is governed primarily by the number of fibres remaining intact within the crack wake [2]. According to the strength criterion, debonding which facilitates the fibre bridging is governed by the ratio between normal debonding stress at the interface and the stress perpendicular to the crack plane in the matrix ligament ahead of the crack tip. Interfacial separation can occur at any time before the crack tip reaches the interface or when the crack is at the interface, provided that the bond strength is lower than a certain fraction of the fibre strength [3–5]. It must be noted that even the strongest interface, which is Ti/SCS 0 system, debonds

F. Kaya (✉)
Department of Metallurgical and Materials Engineering, Faculty of Engineering, Zonguldak Karaelmas University, Zonguldak, Turkey
e-mail: figenkaya81@hotmail.com

before the fibre is fractured, as the debonding stress is approximately 380 MPa and mean fibre strength (measured from the extracted bridging fibres) is 1400 MPa. Interfacial debonding is observed to occur between the carbon coating layers and after interface is debonded, the ability of the fibre to bridge the fatigue crack is determined by the fibre strength relative to the applied stress [3]. Titanium matrix composites reinforced with silicon carbide fibres, either SCS 6 or SM1240 are, characterised by strong fibres, weak interfaces and compressive residual stresses at the fibre matrix interfaces [2]. As the fibre at the crack tip is strong enough to withstand the stress concentration, the fatigue crack propagates around the fibre, causing matrix cracking and fibre/matrix interfacial debonding. In unidirectionally reinforced composite containing holes or notches and loaded along the fibre axis, single-dominant crack propagation located perpendicular to the fibres often takes place [1]. This is accompanied by interfacial debonding ahead of the crack tip and which leads eventually to fibre bridging. When intact fibres bridge a Mode I crack, the crack driving force is shielded by the load carried by bridging fibres. Shielding of crack tip driving forces occurs in two ways. First, the high modulus fibre ahead of the crack tip carries a larger fraction of the load than the matrix, thus reducing the local stress intensity factor at the matrix crack tip slightly, and resulting in a reduced crack growth rate [6]. In order to achieve maximum crack growth resistance, a balance between interfacial strength and fibre bridging must be obtained. Although a weakly bonded interface is desired for increased fatigue crack growth resistance, it also promotes reduced transverse strength, since the transverse strength of composites is determined primarily by the interfacial bonding strength.

The fibre/matrix interface is a critical constituent of composites, as the load transfer from the matrix to the high modulus fibre and vice versa occur through the interface. It is this load transfer behaviour that distinguishes composites from monolithic materials. Interfacial stresses arise from differential thermal contraction and prior plastic flow of the matrix, as well as by the application of an external load. Work carried out on Ti-15V-3Cr/SCS-6 composite shows that repeated sliding of fibre-matrix interfaces which can cause wear of interfaces either by fracture of the coating, asperity wear and/or plastic relaxation of the friction stress on the interface [7]. The large reduction in initial push-out stress of pre-fatigued specimens was again related to diminished misfit strain due to fragmentation of carbon coating. If wear debris is found between mating surfaces then a slight increase in interfacial frictional stress may be rationalised. Guo and Kagawa [8] examined changes of τ_s in a specimen subjected a series of push-out and pushback tests. They found that frictional interfacial shear sliding occurs between unreacted SCS coating layers and the reaction layer. The interfacial shear stress decreases with an increase of push-out/push-back cycles applied. This reduction originates from the abrasive wear of the carbon-rich SCS coating layer by the harder reaction product. Interface wear also varies with test temperature: in a Ti-15V-3Cr-3Al-3Sn/SCS-6 composite system, fine debris was observed at ambient temperature, while at 550 °C two types of wear debris are observed the debonded interface [9]. At elevated temperature, it is observed that the interface shear sliding length and the amount of the wear debris increases with increased numbers of fatigue cycle. The frictional damage of the coating causes a reduction in interfacial shear stress of the composite depending on the maximum applied stress (σ_a) and number of cycles. With an increase of these factors, the interfacial shear stress decreases. The surface damage of fibres, which is introduced by cyclic sliding of bridged fibres appears to have a large effect on fatigue life. Theoretically titanium matrix composites possess fatigue thresholds below which fatigue damage initiation does not occurs [10–15]. However, due to both interfacial and fibre strength degradation the threshold may be shifted to lower applied stresses. If the frictional interfacial stress is assumed to be a function of radial residual stresses around the fibres, then the degradation would be more pronounced when the interface is stronger. In this work, radial stresses around the ceramic fibres are increased via peak ageing in order to investigate the link between radial residual stresses and interfacial strength degradation and fibre strength degradation.

Experimental methods

The material used in this work was Ti β 21 S/SCS 6 composite, with a fibre volume fraction of 35%. The specimens were cut into rectangular bars of dimensions $4 \times 1.75 \times 75$ mm and were heat treated at a temperature of 540 °C for 8 h. Fatigue crack growth resistance tests were conducted on single edge notched specimens in three point bending at ambient and 500 °C both in air and vacuum. In this work a_o/W ratios of 0.24 and 0.07 were used since, these notch sizes were associated with crack arrest and fast failure, respectively, in previous work [16]. All fatigue tests were performed under load control, using 10 Hz frequency and load ratio of $R = 0.5$ ($R = \sigma_{min}/\sigma_{max}$). After cyclic tests, the

pre-fatigued specimens were electro-polished and each fibre was removed taking care to record their position with regard to the initial notch tip. The fibres extracted from the composite were glued along the central line of slotted paper tabs, as shown in Fig. 1a. The paper tabs then were aligned and mounted in the test machine (a part of the fibre was also gripped in order to eliminate the sliding along either fibre/glue interface or between the carbon coating layers, as shown in Fig. 1b. The slot gauge and grip gauge length were controlled to be 20 and 40 mm, respectively and the paper tab was cut within the slot gauge length just before monotonic loading. The single fibre tensile tests were conducted on a servo-hydraulic system equipped with a 1 kN load cell calibrated to a full-scale load range of 100 N. All tests were conducted under a constant piston ramp rate of 0.1 mm/min. The applied load and the displacement of the piston were recorded using an X–Y recorder. The results of the fibres that fractured outside of the slot gauge were discarded. A low bonding strength tape was wrapped around the fibre before loading in order to retain fracture surfaces of the fibres, which were subsequently analysed by using a Field Emission Gun (FEG) Hitachi S4000 scanning electron microscope. The fibre strength distribution was analysed using a tri-modal Weibull function in the form of;

$$F(\sigma_f) = 1 - p.\exp\left\{-\left(\frac{\sigma_f}{\sigma_{01}}\right)^{m1}\right\} - q.\exp\left\{-\left(\frac{\sigma_f}{\sigma_{02}}\right)^{m2}\right\} - r.\exp\left\{-\left(\frac{\sigma_f}{\sigma_{03}}\right)^{m3}\right\} \quad (1)$$

where: $F(\sigma_f)$ is the cumulative failure rate, mi and σ_{0i} (i = 1, 2, and 3 for low, medium and high strength fibres, respectively) are Weibull parameters of each sub-population, and p, q and r, are the percentages of the fibres with these low, medium and high strengths.

Results of the single fibre tensile tests

Composites with an initial unbridged crack size, a_o/W ratio of 0.24

Figure 2 shows the strength distribution of the silicon carbide fibres extracted from unfatigued as- received (AR) and peak aged (PA) Ti β 21S/SCS 6 composites. These results show that the fibre strength ranges between 1000 and 4500 MPa and the ceramic fibres with ultimate tensile strengths higher than 3700 MPa make the larger proportion of the population, compared to fibres with lower tensile strength values. Mean fibre strengths calculated from both composite specimens are observed to be similar, 3620 and 3523 MPa for AR and PA composites, respectively. The Weibull plots of AR and PA composites show that both plots exhibit linear distributions in the region of $\ln(\sigma_F) \geq 8$, (which corresponds to $\sigma_F \geq 3000$ MPa) [Fig. 3]. Both plots also exhibit ''tails'' in the region of $\ln(\sigma_F) \leq 8$, (which represents $\sigma_F \leq 3000$ MPa). Therefore the strength distribution of SCS 6 fibres cannot be expressed adequately by a single Weibull function. Close SEM inspection of the fracture surfaces of the fibres shows that fibres exhibit three distinct types of fracture

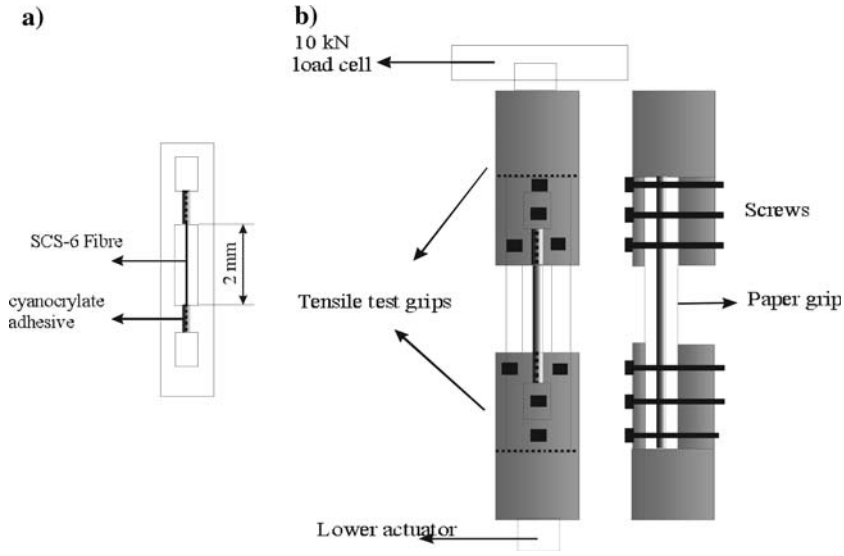

Fig. 1 Schematic diagram showing the single fibre test specimen (**a**) and single fibre tensile loading set up (**b**)

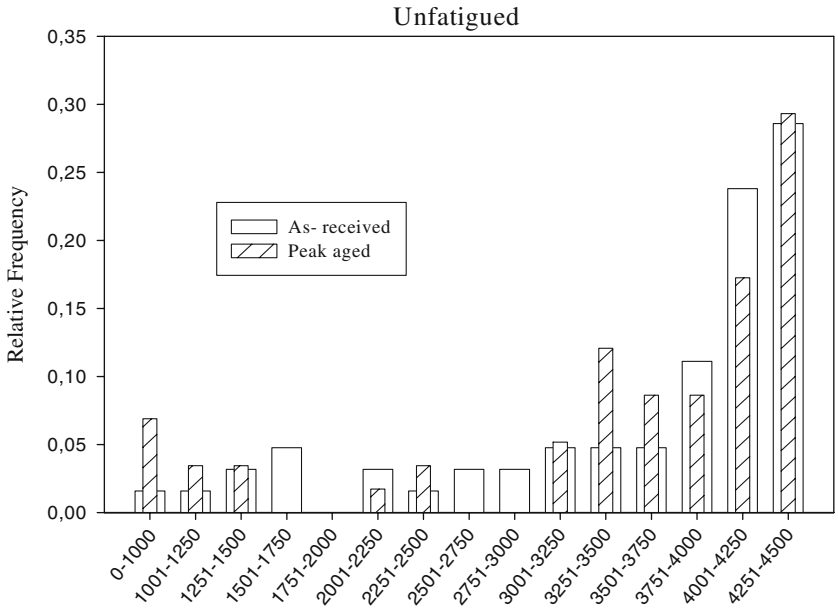

Fig. 2 Strength distributions of the SCS 6 fibres extracted from unfatigued as- received and peak aged Ti β21S/ SCS 6 composites

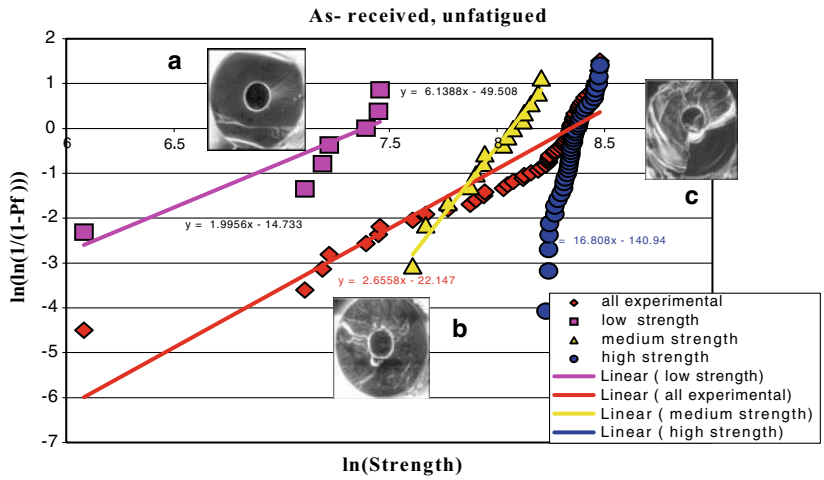

Fig. 3 Weibull plot of SCS 6 fibres extracted from the unfatigued as- received Ti β 21S/ SCS 6 composite. Corresponding fibre fracture surfaces are also illustrated alongside the Weibull distributions of the sub-samples

(a) Low strength fibres ($\sigma_F \leq 2000$ MPa)
(b) Medium strength fibres ($2000 \leq \sigma_F \leq 3700$ MPa)
(c) High strength fibres ($\sigma_F \geq 3700$ MPa)

morphology depending on their tensile strength, as shown in Fig. 3. SEM fractographs of ceramic fibres with tensile strength higher than 3700 MPa exhibit rough fracture morphology with hackles radiating from centre of the fibres, whereas the fracture morphology of the fibres with tensile a strength between 2000 and 3700 MPa are described by fine ridges with some signs of their radiating from the carbon core. Finally for the fibres with tensile strength lower than 2000 MPa, the fracture is observed to start from surface defects. Furthermore when the fibre strength data in the present work are divided into three sub-samples with divisions at 2000 and 3700 MPa, the fibre strength in each sub-sample follows a single Weibull distribution, as shown in Fig. 3. Usage of the multimodal strength distribution is quite common in Ti based metal matrix composites, as chemical reaction between the fibre and matrix, mechanical damage during the consolidation and following heat treatment may introduce surface flaws on the ceramic fibres. Hence, based on the fracture morphology and the results of well defined Weibull distributions of the sub-samples (Fig. 3), the strength distribution of the fibres is divided into three categories in this paper and the validity of this approach is confirmed by the good agreement in probability of failure, P_f, between calculated and experimental

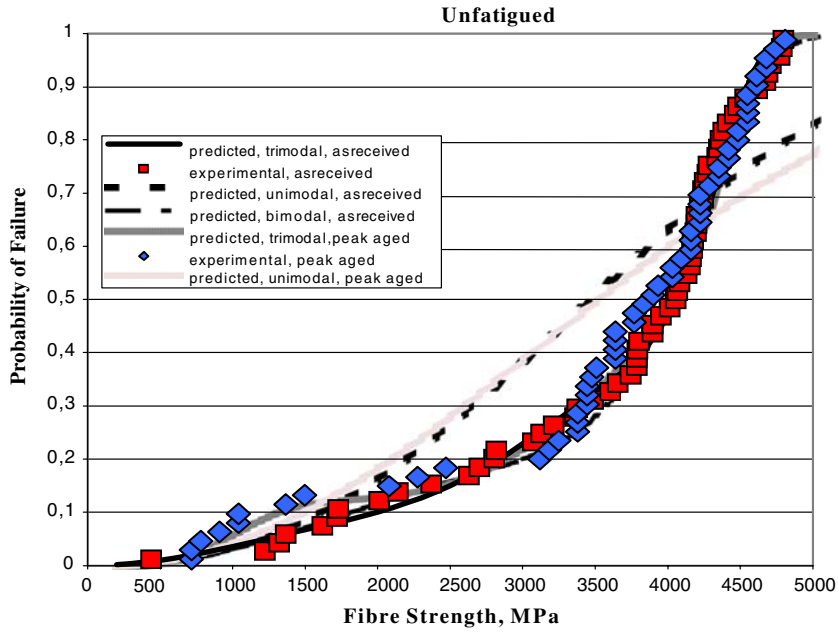

Fig. 4 A comparison of Weibull functions with the experimental results of single fibre tensile tests conducted on the fibres extracted from the unfatigued composites

results, as shown in Fig. 4. Predicted results of the unimodal and bimodal Weibull statistical models are also plotted alongside the tri-modal Weibull model and results show that the tri-modal Weibull model provides a better fit to experimental results, particularly in the high strength region where the single fibre tensile strength, $\sigma_F \geq 3000$ MPa, compared to unimodal and bimodal models (Fig. 4). Fig. 5 shows the probability of failure versus fibre strength plots of unfatigued AR and PA composites. The results show that ageing the Ti β 21S/ SCS 6 composite at 540 °C in an argon atmosphere decreases the fibre strength distributions to some extent in the low strength region ($\sigma_F \leq 2000$ MPa), as compared to the AR composite. More fibres with tensile strength values lower than 1000 MPa are observed in the PA composite. The mean strength of (3523 MPa) the PA composite is observed to be slightly lower than the mean strength of 3620 MPa of the fibres observed in the AR composite, as shown in Table 1. However, overall results suggest that peak ageing at 540 °C in vacuum atmosphere for 8 h does not affect the fibre strength significantly. The mean fibre strength of peak aged specimen pre-fatigued at $K_{max,\ ini} = 25$ MPam$^{1/2}$ is calculated to be 2781 MPa, which is lower than the mean strength (3523 MPa) of the fibres in the un- fatigued PA composite (see Table 1). This suggests that fatigue cycling reduces the fibre strength. The strength distribution of the fibres extracted from the fatigued PA composite reveals that the difference between unfatigued and fatigued fibre strength popu-

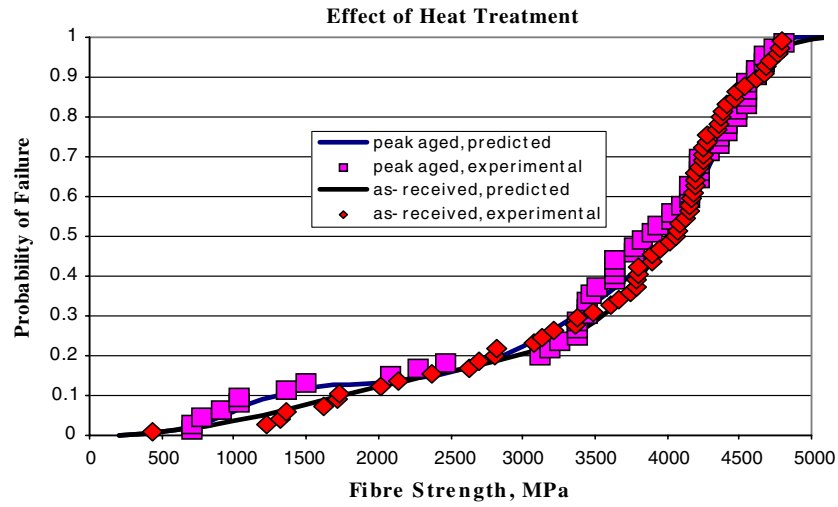

Fig. 5 A comparison between the Weibull statistical models and experimental single fibre tensile tests results of as-received and PA composites

Table 1 Results of the single fibre tensile tests

AR = as- received PA = peak aged	AR	PA	PA K_{max} = 25 MPam$^{1/2}$ a_o/W = 0.24	PA K_{max} = 23 MPam$^{1/2}$ a_o/W = 0.24 (N_f = 1,200,000)			PA K_{max} = 23 MPam$^{1/2}$, a_o/W = 0.24 (N_f = 20,000,000)	PA K_{max} = 21MPam$^{1/2}$ a_o/W = 0.24 (N_f = 23, 000,000)
				All Fibres	Bridging Fibres	Unbridging Fibres		
Mean	3620	3523	2781	2816	2839	2800	2775	2700
Standard Deviation	1043	1176	823	941	879	992	877	811
99%. Conf	349	412	339	318	492	444	370	357
Size	63	58	43	62	25	37	41	40
Minimum	438	715	533	325	325	390	1365	910
Maximum	4800	4810	3900	4420	4420	4425	4160	4160

AR = as-received PA = peak aged	PA K_{max} = 27 MPam$^{1/2}$ a_o/W = 0.07 (N_f = 1,200,000)			PA K_{max} = 23 MPam$^{1/2}$ a_o/W = 0.07 (N_f = 1,100,000)	PA K_{max} = 19 MPam$^{1/2}$ a_o/W = 0.07 (N_f = 950,000)	PA K_{max} = 23 MPam$^{1/2}$ a_o/W = 0.07 (500 °C in vacuum) (N_f = 1,400,000)
	All Fibres	Bridging Fibres	Unbridging Fibres			
Mean	2997	3014	2992	2873	2998	3050
Standard Deviation	1118	967	1169	933	1268	736
99% Conf	310	584	376	253	367	378
Size	92	24	68	94	83	29
Minimum	455	1235	455	65	260	1690
Maximum	4940	4420	4940	4680	5395	4420

Table 2 Statistical results of the pre-fatigued PA composites. Single fibre tensile strength data was divided into two populations, i.e. specimen with an a_o/W of 0.24 and 0.07

	PA a_o/W = 0.24			PA a_o/W = 0.07		
	All Fibres	Bridging Fibres	Unbridging Fibres	All Fibres	Bridging Fibres	Unbridging Fibres
Mean	2760	2074	2816	2848	2759	2870
Standard Deviation	868	848	880	1058	1076	1054
Standard Error	64	99	84	50	113	55
95% Conf	126	198	166	97	224	109
99% Conf	167	263	219	128	297	143
Size	184	73	111	456	91	365
Minimum	325	325	390	65	195	65
Maximum	4420	4420	4225	5395	4420	5395

lations is due to the absence of high strength fibres (≥4000 MPa) in the fatigued composite, as shown in Fig. 6. Indeed the highest fibre strength measured in this particular composite is 3900 MPa, as shown in Table 1. It is observed that the probability of failure vs. fibre strength plots of unfatigued and fatigued PA specimens have different slopes. The good agreement between the predicted and experimental fibre strength data, for both conditions is of particular interest, indicating the validity of the trimodal Weibull function [17]. Fig. 6 shows the tri-modal Weibull distributions of the PA composite tested at $K_{max,\ ini}$ of 25 and 23 $MPam^{1/2}$. The results show that cyclic loading at higher initial applied stress intensity factor values affects the probability of failure versus fibre strength plot in two ways. First the strength of fibres in the high strength region, $\sigma_F \geq 4000$ MPa degrades, as no fibre with tensile strength higher than 4000 MPa is observed in the specimen tested at $K_{max,\ ini}$ of 25 $MPam^{1/2}$. Second, low strength fibres, $\sigma_F \leq 500$ MPa, fracture due to fatigue loading, as no fibre with tensile strength lower than 500 MPa is observed in the PA composite tested at $K_{max,\ ini}$ of 25 $MPam^{1/2}$. Fibre strength distributions of two PA composites tested under fixed $K_{max,ini}$ of 23 $MPam^{1/2}$ to total number of cycles of 1,200,000 and 20,000,000 cycles is shown in Fig. 7. Compared to the PA specimen tested to crack arrest at 1,200,000, fibre strength distribution of the specimen which is tested to crack arrest at 20,000,000 is completely different, as shown in Fig. 8. It is observed that the specimen cycled to 20,000,000 cycles exhibits no fibre with a tensile strength value higher than 4250 MPa or lower than 1250 MPa. Indeed the maximum single fibre tensile strength observed in this particular specimen is 4160 MPa, and the minimum tensile strength is 1365 MPa (see Table 1). However, the mean strengths of the PA specimen cycled to 1,200,000 cycles is measured to be 2816 MPa, whereas the PA specimen that was fatigue tested to 20,000,000 cycles exhibits a mean fibre strength of 2775 MPa, as shown in Table 1. Although, the difference between the two populations is not significant, these results suggest that prolonged fatigue cycling, causes low strength fibres to fracture (as no fibres are detected below 1350 MPa) and increases the probability of failure considerably (for a fixed strength value), between single tensile fibre strength values of 1500 and 3500 MPa. This may suggest that longer fatigue cycling of a composite at lower initial applied stress intensity factor values is more damaging to the tensile strength of the SCS 6 fibres than shorter fatigue loading at higher initial applied stress intensity factor values. This may confirm that, the fibre strength degradation is a time driven process (Fig. 8).

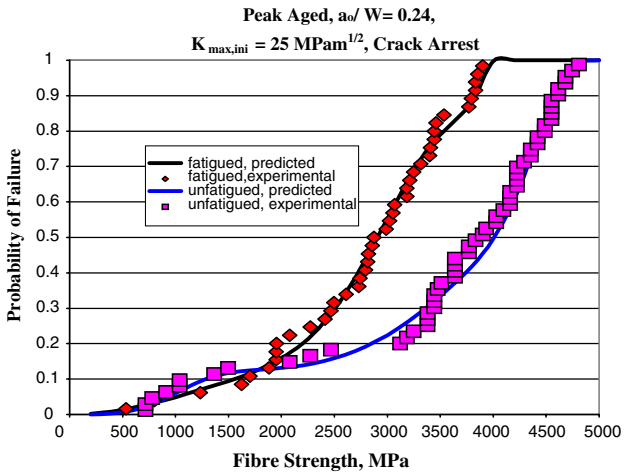

Fig. 6 Probability of failure versus fibre strength plots of the PA composites show that fatigue cycling reduces the fibre strength

Composites with an initial unbridged crack size, a_o/W ratio of 0.07

The fibre strength distribution of fibres from a PA composite fatigue specimen with an initial notch

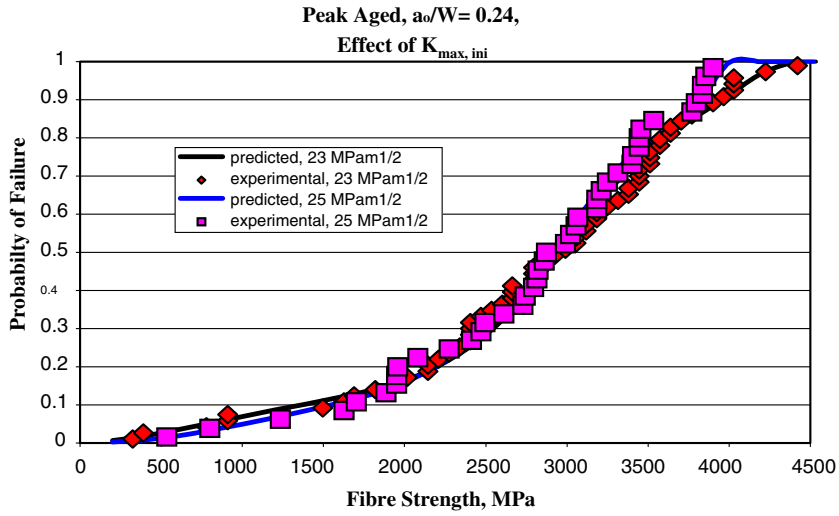

Fig. 7 A comparison of probability of failure versus fibre strength plots of PA composites tested at $K_{max,\ ini}$ of 25 and 23 MPam$^{1/2}$

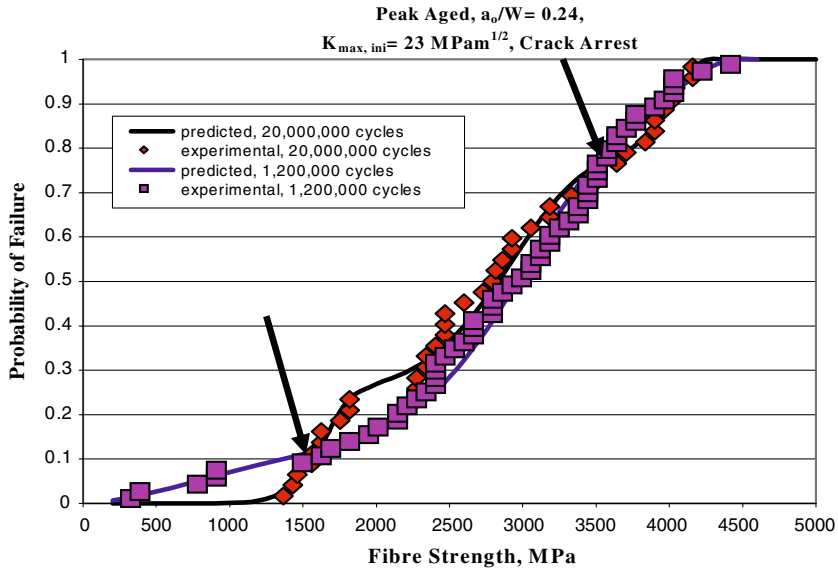

Fig. 8 Tri-modal Weibull plots of PA specimens tested at 23 MPam$^{1/2}$

length to specimen width ratio, a_o/W, of 0.07, tested at $K_{max,\ ini}$ of 27 MPam$^{1/2}$ is shown in Fig. 9. The mean fibre strength of this particular specimen is calculated to be 2997 MPa, which is slightly higher than the mean strength value of 2816 MPa, for the PA composite with a_o/W of 0.24 tested at $K_{max,\ ini}$ of 23 MPam$^{1/2}$, as shown in Fig. 9 and Table 1. Fibre strength distributions of these specimens reveal that the difference is caused by a higher number of fibres with tensile strength values higher than 4000 MPa in the specimen with a shorter notch compared to the fibre strength distribution of the composite specimen with a longer notch, as shown in Fig. 9. Indeed, the maximum and minimum single fibre tensile strengths observed in the former specimen are 4940 and 455 MPa, whereas the maximum and minimum tensile strengths observed in the latter specimen are 4420 and 325 MPa (see Table 1). As no marked effect of the initial notch depth to specimen width, a_o/W is observed on the fibre strength distributions, the tensile fibre strength data of the PA composite which are tested to crack arrest under $K_{max,ini}$ of 23 and 27 MPam$^{1/2}$ are divided into two populations (i.e. bridging fibres which were previously located within the crack wake and the un-bridging fibres, which were located outside of the fatigue crack wake) as shown in Figs. 10 and 11. When the strength distributions of the fibres which were originally located within the crack wake compared it is observed that for the fibre strength values smaller than 2400 MPa, the probability of failure is higher for the specimen with a_o/W of 0.07 (for a fixed fibre strength) and this difference is greater in the fibre strength region where $2500 < \sigma_F < 1500$ MPa, as shown (marked with the arrows) in

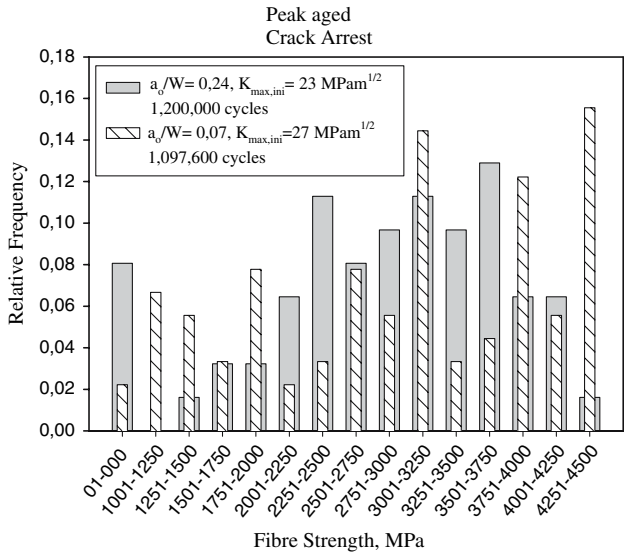

Fig. 9 Fibre strength distribution of a PA composites with initial notch length to width ratios of 0.07 and 0.24. Composites were pre-fatigued to crack arrest at at 27 and 23 MPam$^{1/2}$ respectively

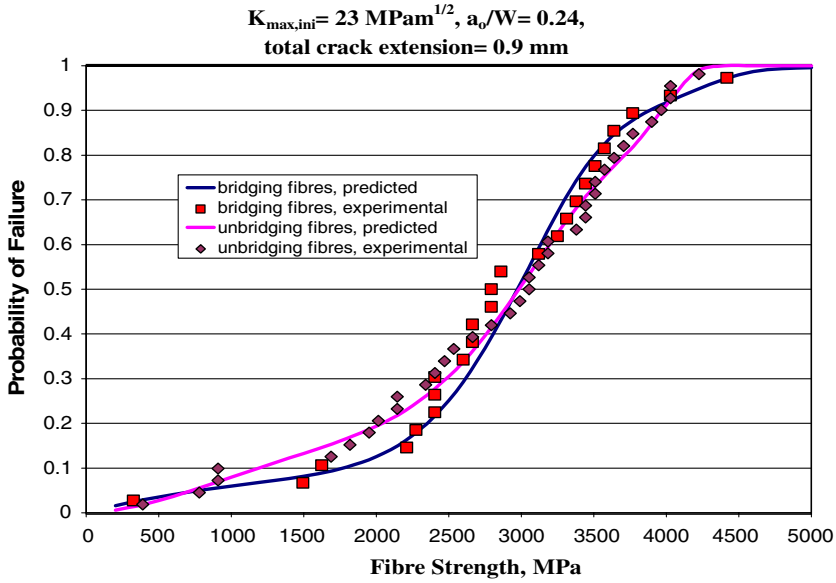

Fig. 10 A comparison of the bridging and un-bridging fibres extracted from a PA composite with a_o/W of 0.24 tested at $K_{max,ini}$ of 23 MPam$^{1/2}$

Fig. 12. Results show that SCS 6 fibres in the specimen with a_o/W of 0.07 that was pre-fatigued at an initial K_{max} of 27 MPam$^{1/2}$, is much stronger than the fibres in the specimen with a_o/W of 0.24, which is prefatigued at $K_{max,\ ini}$ of 23 MPam$^{1/2}$. This may explain the reason for crack arrest being observed at a higher initial maximum applied stress intensity factor value for a specimen with smaller initial notch length. Previous work [16, 18] has shown that in general under a fixed initial maximum applied stress intensity factor value, $K_{max,\ ini}$, the fatigue crack growth rate in a composite with a smaller notch is much higher and the catastrophic failure occurs after fewer cycles than in the composite with a large initial notch. In contrast to previous results observed by Fox and Cardona et al. [16, 18], in this study a composite specimen with a small notch size, a_o/W, of 0.07 is observed to lead to crack arrest at a high initial maximum applied stress intensity factor, $K_{max,\ ini}$, of 27 MPam$^{1/2}$. Catastrophic failure is observed for a specimen with a longer initial notch size, a_o/W, of 0.24 tested at the same $K_{max,\ ini}$ value (Fig. 13). Results of the single fibre tensile test of this particular specimen ($a_o/W = 0.07$ crack was arrested at $K_{max,\ ini}$ of 27 MPam$^{1/2}$) reveal that the mean fibre strength (in the bridged region is approximately 6% higher than

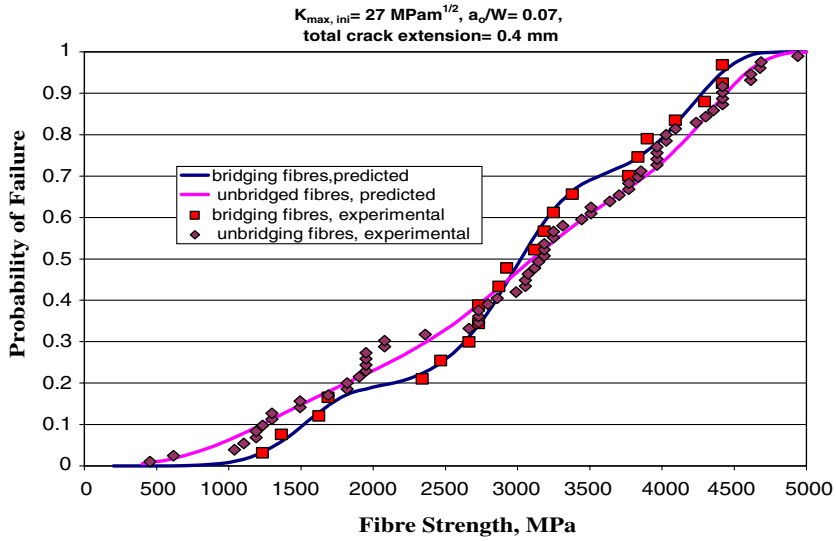

Fig. 11 A comparison of the tri-modal probability of failure plots of the bridging and un- bridging ceramic fibres extracted from a PA composite with a_o/W of 0.07, pre-fatigued at $K_{max,ini}$ of 27 MPam$^{1/2}$

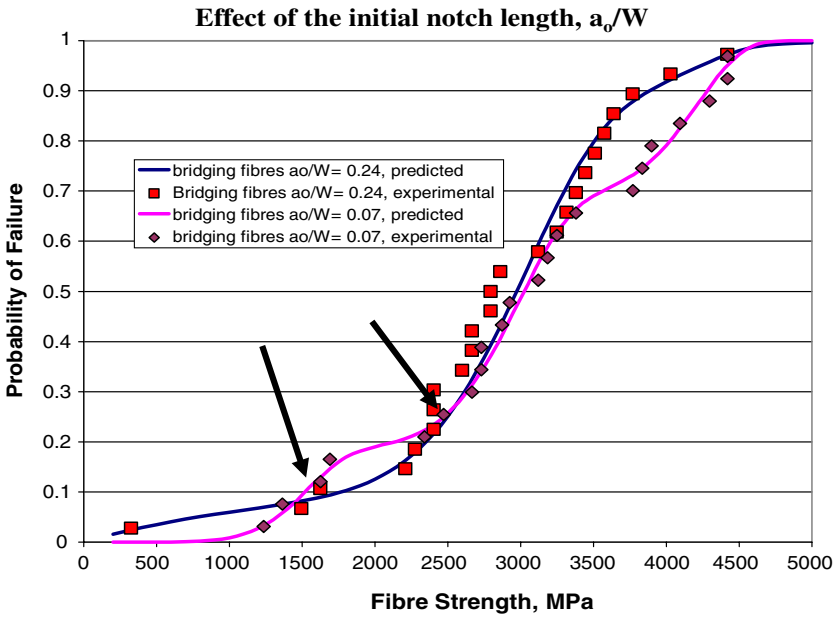

Fig. 12 Probability of failure plots of SCS 6 fibre extracted from the fatigue crack wake of the crack arrest specimens with a_o/W of 0.24 and 0.07 tested at 23 and 27 MPam$^{1/2}$ respectively

that of the specimen which is tested to crack arrest at $K_{max,\ ini}$ of 23 MPam$^{1/2}$ (a_o/W = 0.24). where the mean strength of the bridging fibres of the specimen with the initial notch length of 0.3 mm is calculated to be 3014 MPa, whereas the mean strength of the specimen with the initial notch length of 1 mm is calculated as 2839 MPa (Table 1). This result may indicate the importance of the in situ tensile strength of the ceramic fibres. If a relatively low number of fibres are fractured at the beginning of the fatigue cycling, the fatigue crack growth is controlled by the stress intensity factor value operating at the matrix crack tip and for a fixed crack length, the effective crack tip stress intensity factor value is smaller. Therefore both fatigue crack growth rate and the crack length needed to get crack arrest are smaller in specimens with a shorter notch (Table 2).

Figure 14 shows the fibre strength distributions of the SCS 6 fibres extracted from PA composites with a_o/W of 0.07, tested at $K_{max,\ ini}$ of 23 and 19 MPam$^{1/2}$ to crack arrest at 1,070,900 and 3,298,493 cycles, respectively. The mean fibre strength is calculated to be 2873 MPa for the former specimen, which is again slightly lower than the mean fibre strength of 2998 MPa, observed in the latter specimen, as shown in Table 1. This may suggest that, the fibre strength

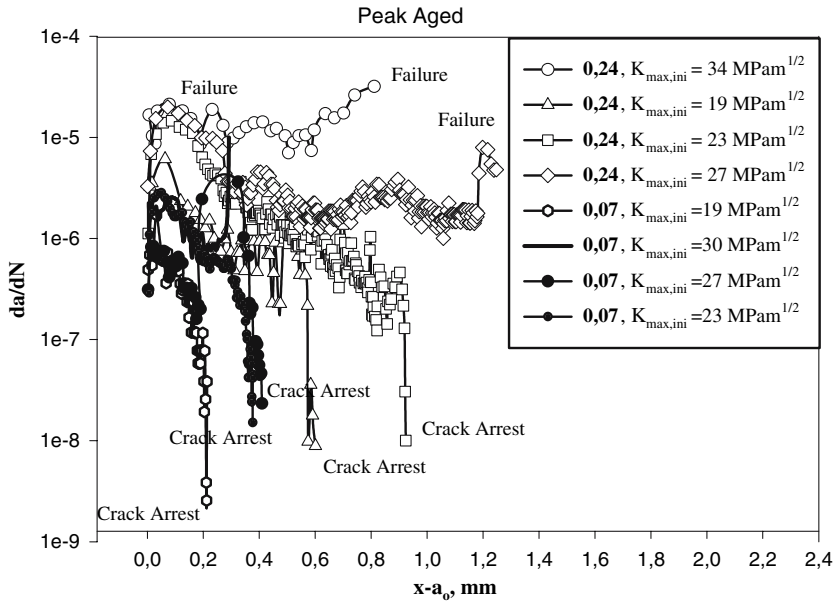

Fig. 13 da/ dN plots of PA specimens with a_o/W:0.24 and a_o/W:0.07

degradation is influenced by the initial maximum applied stress intensity factor value, $K_{max,\ ini}$, as well as the total number of the cycles, N_f. It can be seen that compared to the specimen tested at $K_{max,\ ini}$ of 19 MPam$^{1/2}$, the probability of failure is higher (for a fixed fibre strength value) in the high strength region ($\sigma_f \geq 2500$ MPa) for the fibres extracted from the specimen tested at the higher initial applied stress intensity factor value of 23 MPam$^{1/2}$. It is also observed that low strength fibres fracture when the composite is fatigued at high initial applied stress intensity factor values, as no fibres with tensile strength value lower than 1000 MPa are observed in the specimen tested at $K_{max,\ ini}$ of 23 MPam$^{1/2}$, as shown in Fig. 14.

Conclusions

In general the mean tensile strength of the fatigued fibres was observed to be falling between 2700 and 2900 MPa. Hence, in terms of the mean fibre strength no marked effect of the maximum applied stress intensity value, $K_{max,ini}$, total number of cycles and testing temperature was observed on the fibre strength degradation. Therefore the single fibre tensile test results data were divided into two populations in terms of the initial notch length to specimen width, a_o/W. Statistical analysis of these two populations shown that the mean fibre strengths of the bridging fibres were different and the *t*-test performed on the two populations had confirmed that two populations

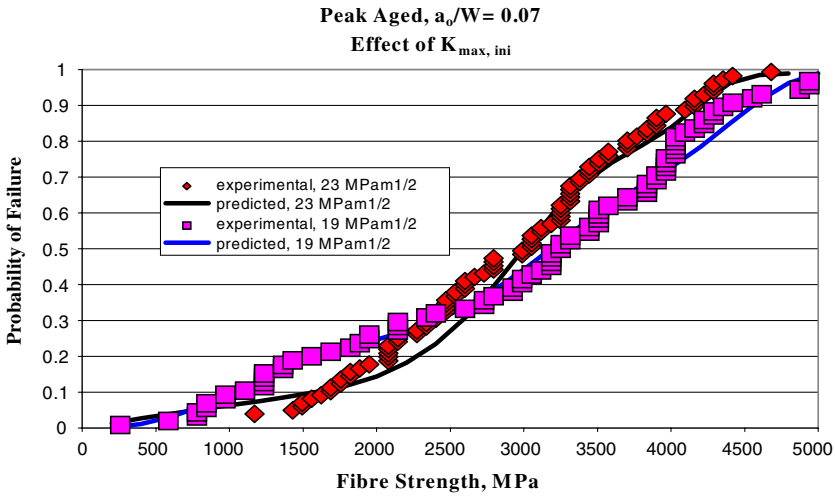

Fig. 14 Probability of failure versus fibre strength plots of the PA composites tested at 23 and 19 MPam$^{1/2}$ to crack arrest at 1,070,900 and 3,298,493 cycles, respectively

were significantly different. Result had shown that the fatigue testing degraded the tensile strength of the bridging fibres significantly, where the mean tensile strength of the bridging fibre extracted from the specimens with a_o/W of 0.24 was measured to be 2074 MPa, whereas the mean tensile strength of the bridging fibres extracted from the specimens with a_o/W of 0.07 was calculated to be 2848 MPa which corresponds to fibre strength reductions of 41 and 22%, respectively (compared to the mean tensile strength of 3523 MPa of the unfatigued fibres). In the unbridging region, however the mean tensile strength were calculated to be similar for both initial notch length which were 2816 and 2759 MPa (which corresponds to strength degradation of 25%), indicating the effect of the initial notch size is only evident on the bridging fibres.

References

1. Bowen P (1992) The processing, Properties and Applications of Metallic and Ceramic Materials II. Proceedings of the International Conference Held at the ICC, Birmingham, UK, 7–10 September, 697–718
2. Majumdar BS (1998) Titanium Matrix Composites, Mechanical Behaviour. In: Mall S, Nicholas T (eds) Technomic Publication, Pennsylvania, 118–126
3. Warrier SG, Majumdar BS (1999) Metall Mater Trans A 30A:277
4. Calcaterra JR, Mall S (1999) Int J Fatig 21(3):215
5. Warrier SG, Maruyama B, Majumdar BS, Miracle DB (1999) Mater Sci Eng A 259(2):189–200
6. Warrier SG, Majumdar BS, Miracle DB (1997) Acta Mater 45:4969
7. Warren PD, Mackin TJ, Evans AG (1992) Acta Metall Mater 40:1243
8. Guo SQ, Kagawa Y (1997) Acta Mater 45:2257
9. Tanaka Y, Kagawa Y, Masuda C, Liu YF, Guo SQ (1999) Metall Mater Trans A 30:221
10. Wang PC, Jeng SM, Yang JM, Mal AK (1996) Acta Mater 44(3):1097
11. Wang PC, Yang JM (1997) Mater Sci Eng A 222(2):101
12. Iyengar N, Curtin WA (1997) Acta Mater 45(4):1489
13. Wang PC, Her YC, Yang JM (1998) Mater Sci Eng A 245(1):100
14. Mcdonnell P (2001) PhD Thesis, The University of Birmingham
15. Zamperini S (2002) PhD Thesis, The University of Birmingham
16. Fox KF (1994) PhD Thesis, The University of Birmingham, UK
17. Kaya F (2003) PhD Thesis, The University of Birmingham, UK
18. Cardona DC, Barney C, Bowen P (1996) Life Prediction Methodology for Titanium Matrix Composites''. In: Johnson WS, Larsen JM and Cox BN (eds) ASTM STP 1253, pp. 164